Analytica Chimica Acta 887 (2015) 192–200

Contents lists available at ScienceDirect

Analytica Chimica Acta

journal homepage: www.elsevier.com/locate/aca

Enhanced immunoassay for porcine circovirus type 2 antibody using enzyme-loaded and quantum dots-embedded shell–core silica nanospheres based on enzyme-linked immunosorbent assay

Long Wu, Xuepu Li, Kang Shao, Shiyi Ye, Chen Liu, Chenjun Zhang, Heyou Han*

State Key Laboratory of Agricultural Microbiology, College of Science, Huazhong Agricultural University, Wuhan 430070, PR China

HIGHLIGHTS

- A versatile ELISA-based immunoassay for PCV2 antibody was developed.
- Enzyme and CdSe QDs modified SiO_2 particles were used to improve sensitivity.
- The simultaneous three ELISA-based techniques enhanced the detection reliability.
- The biosensors strategy could provide a new avenue to ELISA-based sensors.

GRAPHICAL ABSTRACT

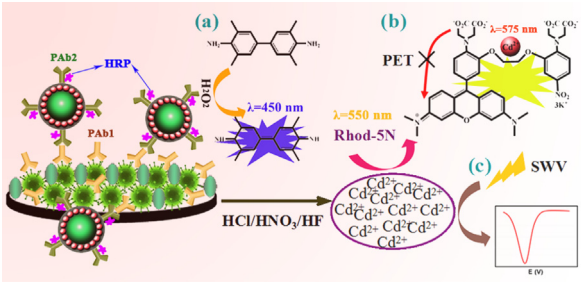

ARTICLE INFO

Article history:
Received 23 March 2015
Received in revised form
21 May 2015
Accepted 11 June 2015
Available online 6 August 2015

Keywords:
Enzyme-linked immunosorbent assay
Immunosensor
Enzyme
Quantum dots
Silica nanosphere

ABSTRACT

Boosting the detection sensitivity of enzyme-linked immunosorbent assay (ELISA) is significant to the early clinical diagnosis of various diseases. Here, we developed a versatile immunosensor using silica nanospheres as carriers for sensitive detection of porcine circovirus type 2 (PCV2) antibody. With HRP enzyme covalently immobilized on the silica nanospheres and CdSe nanocrystals embedded inside, these signal probes were successfully utilized in the sensitive detection of PCV2 antibody by ELISA, fluorometry and square-wave voltammetry (SWV). To further demonstrate the performance of the immunosensor, Human IgG (HIgG) was used as a model analyte. Since more HRP and CdSe QDs were loaded, 5-, 200- and 400-fold enhancements in amplified ELISA, fluorometry and voltammetry responses for HIgG could be achieved compared to conventional ELISA. The respective detection limits of theses methods for HIgG were 3.9, 0.1 and 0.05 ng mL^{-1} with a RSD below 5% for amplified ELISA, fluorescence and SWV measurements. Additionally, a 100-fold improvement was obtained in the detection sensitivity for PCV2 antibody immunoassay. The versatile immunosensor exhibits good sensitivity, stability and reproducibility, suggesting its potential applications in clinical diagnostics.

1. Introduction

Porcine circovirus type 2 (PCV2), the primary causative agent of porcine circovirus-associated disease (PCVAD) and porcine circovirus disease (PCVD), is the smallest virus known to infect mammals [1]. Since it was firstly discovered in 1998, PCV2 has continued to be a virulent swine pathogen causing great economic losses in the swine industry worldwide [2]. Therefore, it is imperative to develop an accurate and sensitive method to implement the early diagnosis. Recently, many methods have been developed to

* Corresponding author.
E-mail address: hyhan@mail.hzau.edu.cn (H. Han).

http://dx.doi.org/10.1016/j.aca.2015.06.024
0003-2670/

diagnose various diseases, including Enzyme-linked immunosorbent assay (ELISA) [3], radioimmunoassay [4], fluorometric enzyme immunoassay (FEIA) [5], chemiluminescence immunoassay and Surface enhanced Raman scattering (SERS) [6,7]. Among the various strategies, ELISA has attracted the most interests due to its simplicity and ease of operation and control. However, the relatively low sensitivity is the main limitation of conventional ELISA, which has constrained its application to the early disease diagnosis [8,9]. To resolve the difficulty, great efforts have been made in developing more sensitive immunosensors by introducing sensitive substrates or employing different detection technologies. The innovated techniques include bio-bar-codes assay [10,11], optical methods [12,13], and electrochemical immunoassay [14]. Compare with the conventional ELISA, it still remains challenges in the detection of PCV2 antibody with sensitivity. Therefore, it is of great importance to establish more sensitive and reliable methods for the detection of PCV2 antibody.

Due to the convenient surface modification, quantum dots are popular in the construction of signal amplification strategies coupled with other techniques [15–18]. For example, based on antibody–antigen reaction, a novel versatile immunosensor was developed for the detection of carcino-embryonic antigen using QDs coated silica nanosphere as probes [19]. Meanwhile, the immunoassay for porcine pseudorabies virus (PrV) antibody was developed by fluorescence signal amplification of cation exchange in CdSe nanocrystals [20]. On the other hand, the previously reported work also demonstrated that a stable and homogeneous sandwich type of silica nanosphere probes (SiO_2@QDs@SiO_2) could be successfully obtained by the assembly of QDs with silica substrates [21,22]. With the coating of silica shell, the loading amount of QDs was largely preserved, which further promoted the signal intensity and stability. Besides, the silica shell provided an excellent interface for surface bio-modification due to its facile chemical processability and good stability in aqueous media [23,24]. All these examples indicate that silica nanosphere and QD are great carriers and amplification factors in both the recognition and transduction events.

Herein, we present a versatile detection for PCV2 antibody using enzyme-loaded and CdSe QDs-coated silica nanospherial as probes on the basis of ELISA (see Fig. 1). As shown in Fig. 1A, silica nanoparticles (silica NPs) were firstly employed as carriers for loading CdSe QDs, then HRP labeled secondary antibody (PAb2) was covalently bound to the surface after silica coating (SiO_2@CdSe@SiO_2). Fig. 1B illustrates the detection process for PCV2 antibody via three techniques: ELISA (a), fluorometry (b) and SWV (c). First, PCV2 were immobilized on the 96-well plate after BSA blocking, and then amplified ELISA detection of PCV2 antibody was achieved by a sandwich assay using PCV2 antibody and secondary antibody (PAb2) loaded on the silica nanoparticles. After that, the acid solution (v/v, HNO_3: HF: HCl = 1:1:3) were added into the plate wells, then Cd (II) ions were released from CdSe QDs and further acted as amplified signals to quantify the analyte. The amount of Cd^{2+} was finally quantified by fluorometry (b) and SWV (c), respectively, which increased with the concentration of PCV2 antibody in a certain range. The proposed strategy has been successfully applied in the detection of PCV2 antibody in clinical serum samples, and the results demonstrated the advantages such as good stability and reproducibility and high sensitivity. Thus, the specific strategy would provide precise and sensitive detection of PCV2 antibody but also illuminate biosensor strategy to electrochemistry and fluorescent imaging.

2. Material and methods

2.1. Chemicals and materials

Tetraethyl orthosilicate (TEOS, 99%), 3-(Glycidyloxypropyl)trimethoxysilane (GPTMS, ≥95%), (3-Mercaptopropyl) trimethoxysilane (MPTS, 95%), sodium silicate solution (SiO_2, wt 27%), bovine serum albumin (BSA), trioctylphosphine oxide (TOPO, 90%), hexadecylamine (HDA, 90%), stearic acid (SA, 95%), cadmium oxide (CdO, 99.99%), dioctylamine (DOA, 90%), mercaptopropionic acid (MPA, 99%) and selenium powder (99.99%) were purchased from Sigma–Aldrich; N-octyltrimethoxysilane (OTMS, 97%) was

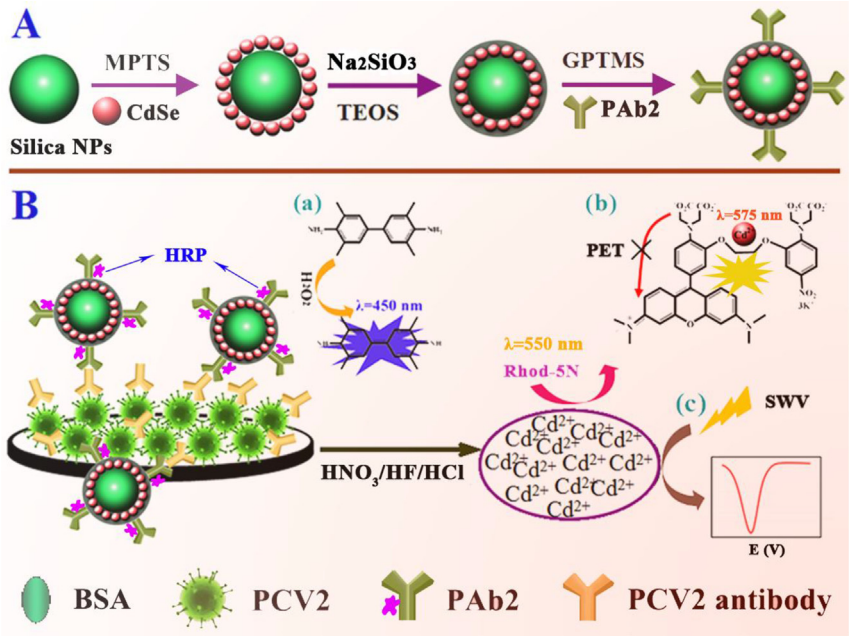

Fig. 1. Schematic illustration of the versatile immunosensor, (A) the enzyme-loaded and signal-coated process of silica nanosphere label, and (B) the immunoassay process for PCV2 antibody based on ELISA, fluorometry and voltammetry (SWV).

supplied by Alfa Aesar; Rhodamine 5 N (Rhod-5N) was purchased from Invitrogen Corporation of California; Tween-20, ethanol, toluene, chloroform and other relevant reagents were obtained from Sinopharm Chemical Reagent Co. Ltd.; All chemicals and solvents were of analytical grade and used as received without further purification.

Human IgG antigen (HIgG, 50 mg mL^{-1}), rabbit anti-human IgG antibody (HAb1, 1 mg mL^{-1}), HRP-conjugated goat anti-human IgG antibody (HAb2, 0.1 mL mL^{-1}), HRP-conjugated rabbit anti-pig IgG antibody (PAb2, 1 mg mL^{-1}) were obtained from Sangon Biotech Co., Ltd. (Shanghai, China); PCV2 antibody (PAb1), positive and negative serum of PCV2 packaged in the PPA-ELISA kits were from Shandong Lvdu Bio-science & Technology Co. Ltd; The polystyrene 96-well plates, PrV and Porcine Reproductive and Respiratory syndrome (PRRS) positive serum were acquired from Wuhan keqian Animal Biological Products Co. Ltd.

Ultrapure water obtained from a Millipore water purification system (Milli-Q, Millipore, 18.2 MΩ resistivity) was used throughout the experiment.

2.2. Instrumentation

All the samples and immunoassay procedure were coated and performed on the 96 well plates; Fluorescence and optical density (OD) measurements were operated on Perkin Elmer 1420 Multilabel Counter; Photoluminescence (PL) spectra were measured on Edinburgh FLS920 spectrometer under excitation of 550 nm light; Square-wave voltammetry (SWV) was performed by an electrochemical work station (CHI660D Instruments, Shanghai Chenhua Instrument Corp., Shanghai, China).

The UV–vis absorption spectra were obtained on Nicolet Evolution 300 UV–vis spectrometer (Thermo Nicolet, America); Fourier transform infrared (FT-IR) spectra were acquired on a Nicolet Avatar-330 spectrometer with 4 cm^{-1} resolution using the KBr pellet technique; Transmission electron microscopy (TEM) images were collected by a JEM-2010 transmission electron microscope (JEOL, Japan); Hydrodynamic diameters were measured by using dynamic light scattering (DLS) technique on Malvern Zetasizer Nanoseries (Malvern, England) with 633 nm laser excitation at 25 °C.

2.3. Preparation of SiO_2@CdSe@SiO_2 probes

Firstly, silica nanospheres were prepared according to the procedures described in literature with additional modifications [25]. The obtained solution was centrifugated to remove excess reactant and the precipitate was resuspended in ethanol. Secondly, CdSe QDs were assembled onto the silica nanospheres to produce CdSe QDs loaded SiO_2 after the process of sulfhydrylation. Thirdly, the obtained SiO_2@CdSe was reacted with OTMS and sodium silicate solution for silica coating. Finally, SiO_2@CdSe@SiO_2 probes were synthesized by epoxy-functionalization and then conjugated with antibody based on the previous method [21,26,27]. The schematic illustration was shown in Fig. 1A and the detailed procedures were provided in Supplementary Information.

2.4. Sandwich ELISA of HIgG and PCV2 antibody

The whole fabrication process of 96-well plate was illustrated in Fig. 1B (a). HIgG was selected as a model analyte and finally recognized with HAb2 which was loaded on SiO_2@CdSe@SiO_2 probes to produce amplified optical signal. As shown in Fig. 1B, the same procedures were adopted for the detection of PCV2 antibody. The detailed procedures were specified in Supplementary Information.

2.5. Fluorescence detection and SWV analysis

The enzyme-loaded probes were subsequently used to provide Cd^{2+} originated from the coated CdSe QDs. Typically, 50 μL of the mixed acid solution (v/v, HNO_3: HF: HCl = 1:1:3) was added to each coated well and shaken for 10 min on a shaking incubator. Then, a saturated solution of sodium hydroxide was drop-wise added until a pH of 7.0 was reached. Finally, 0.1 M phosphate buffered saline solution (PBS, pH = 7) containing 4.0 μM Rhodamine 5 N was added for the fluorescence measurement.

For the voltammetric analysis, the pH of acid dissolved probes was adjusted to 5.3, and then the resulting solution was mixed with 0.2 M HAc-NaAc buffer (pH = 5.2) to a final volume of 3 mL [28]. Finally, the SWV analysis was performed with a conventional three-electrode system comprised of platinum wire as auxiliary electrode, Ag/AgCl (saturated KCl) electrode as reference.

3. Results and discussions

3.1. Characteristics of silica spheres

The uniformity and stability of silica spheres are fundamental to the construction of SiO_2@CdSe@SiO_2 probes, which may have great influence on the reproducibility, sensitivity, and analytical performance of the resultant immunosensor. It is for this reason that the seed-growth method was chosen to synthesize the silica spheres with the size of 90 nm [29]. The modification processes of silica spheres were monitored by FT-IR spectra, UV–vis absorption spectra, PL spectra, TEM and DLS.

As depicted in the FT-IR spectra (see Fig. 2A), the absorption bands at 467 cm^{-1} (Si–O), 796 cm^{-1} (–OH), and 953 cm^{-1} (Si–OH) corresponded to the characteristic bands of silica, indicating the same groups on the surface of SiO_2 sphere and SiO_2@CdSe@SiO_2 spheres. However, the decrease of the wide and strong absorption band at 1093 cm^{-1} (Si–O–Si) in curve c indicated the successful silica coating of SiO_2 sphere.

The as-prepared CdSe QDs and silica-based materials were characterized by UV–vis absorption spectrum as shown in Fig. 2B. The CdSe QDs (curve a) showed a strong absorption peak at 560 nm caused by surface plasmon resonance. The dramatic decline of the adsorption peak at 560 nm indicated the successful assembly of CdSe QDs onto silica nanospheres (curve b). After silica coating and epoxidation, the characteristic peak of CdSe QDs was nearly disappeared (curve c and d). PL spectra were used to characterize the as-prepared materials as depicted in Fig. 2C. The PL emission peak of CdSe QDs was at 570 nm with a yellowishgreen emitting light. After the loading of CdSe QDs on the silica sphere, the emission peak behaved a red-shift and the PL intensity enhanced strongly (curve b). However, the following silica coating and epoxidation (curve c and d) quenched the fluorescence of CdSe QDs to a large extent.

Fig. 2D showed the zeta potential of different silica spheres with the average value below −36 mV, demonstrating the stability of the nanospheres. The thin silica layer strengthened the surface charge of SiO_2 spheres with an average zeta potential of −47.6 mV, which would contribute to the epoxidation of SiO_2@CdSe@ SiO_2.

TEM images in Fig. 3A revealed that the synthesized silica nanospheres were uniform and well-dispersed with an average diameter of approximately 90 nm. Moreover, the representative TEM and HRTEM images showed that numerous and individual particles were thickly dotted on silica nanospheres (Fig. 3B and C), indicating the homogeneous distribution of CdSe QDs on the silica nanosphere. Though the featureless silica coating layer and enzyme modification could be hardly identified, a thin layer of colloid shell and fibroid conjugation could be recognized in Fig. 3D and E.

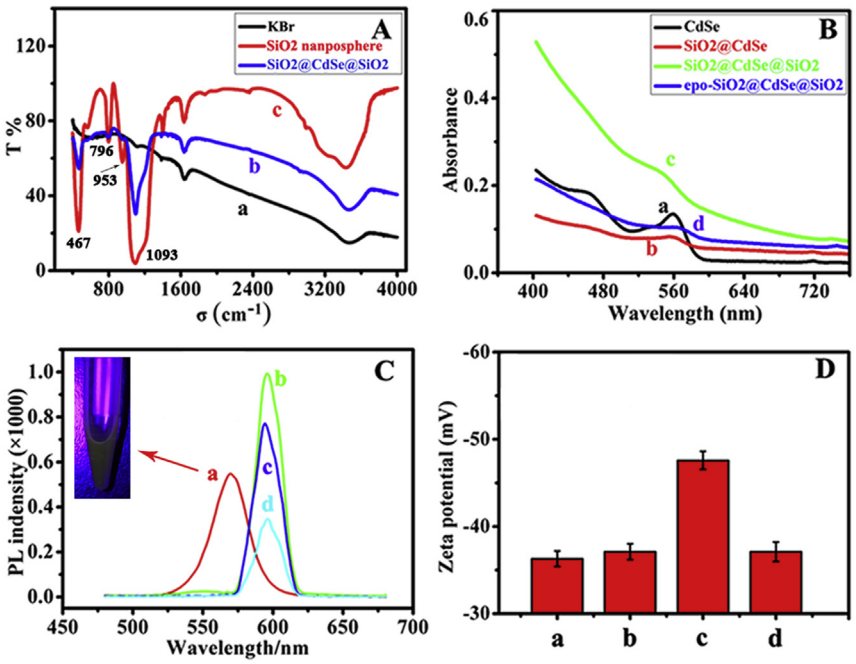

Fig. 2. (A) FT-IR spectra of (a) CdSe QDs, (b) SiO_2@CdSe@SiO_2 spheres, and (c) SiO_2 spheres. (B) UV–vis absorption spectra and (C) PL spectra of (a) CdSe QDs, (b) SiO_2@CdSe, (c) SiO_2@CdSe@SiO_2 spheres and (d) epoxy SiO_2@CdSe@SiO_2 spheres. (D) Zeta potential measurements of (a) SiO_2 spheres, (b) thiolated SiO_2 spheres (c) SiO_2@CdSe@SiO_2 spheres and (d) epoxy SiO_2@CdSe@SiO_2 spheres. All the error bars were calculated based on the standard deviation of three measurements.

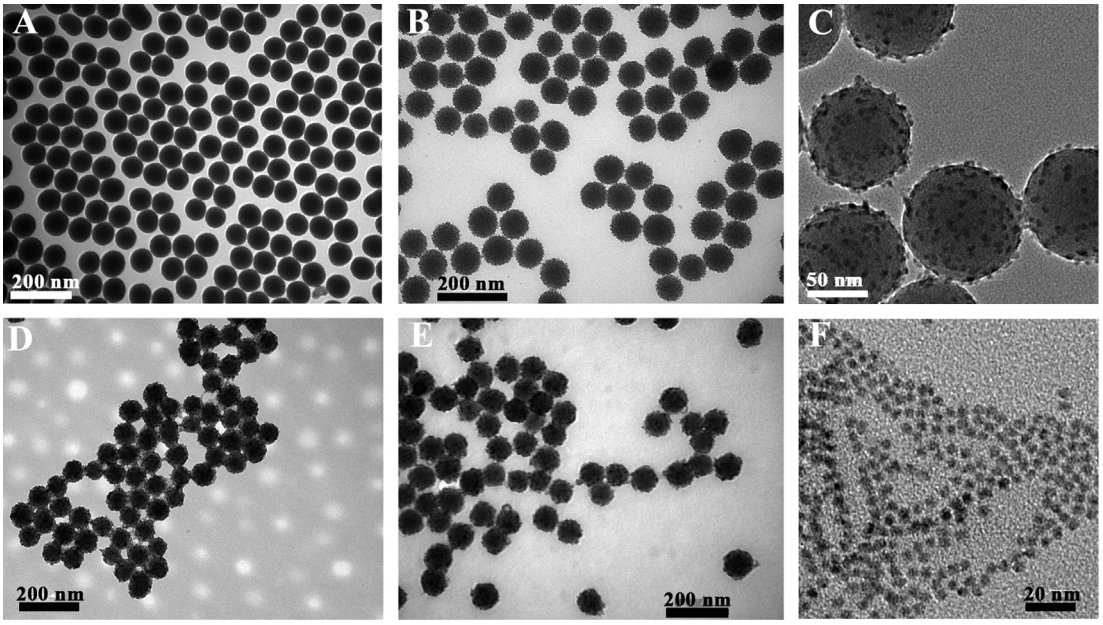

Fig. 3. TEM images of (A) silica nanospheres, (B) SiO_2@CdSe, (C) a zoomed in version of SiO_2@CdSe, (D) SiO_2@CdSe@SiO_2, (E) SiO_2@CdSe@SiO_2-Ab2, and (F) CdSe QDs.

Furthermore, the features could also be distinguished more clearly through the surface identification (see Fig. S1).

Fig. S2 exhibited the hydrodynamic diameters of CdSe QDs and silica nanospheres in different stages. It can be seen from Fig. S2A that the average size of CdSe QDs is about 3.29 nm in diameter with narrow monodispersity, which is consistent with the result of TEM (Fig. 3F). After different procedures, the average hydrodynamic size of silica nanospheres increased from the initial 90.23 nm–118.45 nm (Fig. S2B). The size change reflected that the CdSe QDs were loaded on silica spheres (from 90.23 to 97.04 nm) and HAb2 was successfully modified on the surface of SiO_2@CdSe@SiO_2 (from 100.20 to 118.45 nm). The results further verified the previous conclusions, and the other information can also be obtained from the zeta potential described in Fig. 2D. All these facts confirmed that silica coating of SiO_2@CdSe was accomplished and HAb2 was successfully modified onto the surface of SiO_2@CdSe@SiO_2.

3.2. Characteristics of the immunosensor

As depicted in Fig. 4, the color change of the SiO_2@CdSe@SiO_2-HAb2 and their response to the centrifugation indicated the success

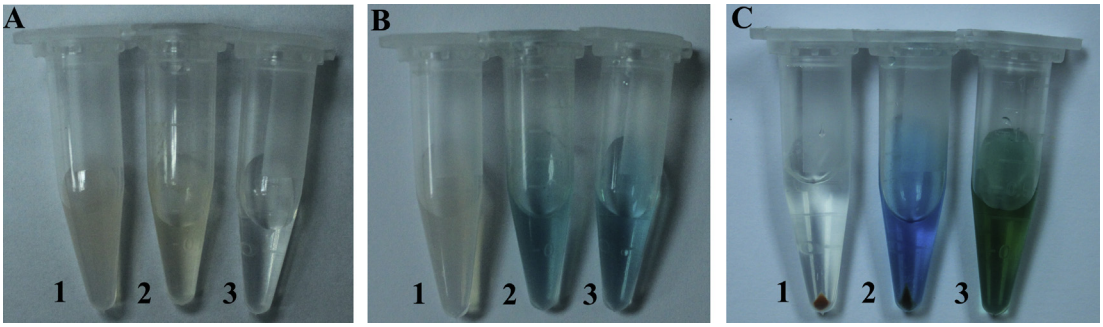

Fig. 4. (A) States of SiO_2@CdSe@SiO_2 spheres before and after immobilization of HRP (1: SiO_2@CdSe@SiO_2 spheres; 2: SiO_2@CdSe@SiO_2 probes; 3: Free HRP). (B) The color change of particles after adding TMB/H_2O_2 and (C) their response to centrifugation without addition of stop solution (correspond to A). (For interpretation of the references to colour in this figure legend, the reader is referred to the web version of this article.)

of HAb2 immobilization. Compared to the states in Fig. 4A, the color of the probes and the free HRP both changed to blue after introducing TMB/H_2O_2 substrates (Fig. 4B). However, the free HRP still remained well dispersed and the SiO_2@CdSe@SiO_2 probes precipitated to the bottom after centrifugation (Fig. 4C). These results revealed that the enzyme activity remained well after the modification, which is crucial to obtain reliable results in the practical applications.

To further investigate the stability of the SiO_2@CdSe@SiO_2 probes, the as-prepared SiO_2@CdSe@SiO_2-HAb2 was centrifuged after 24 h and 72 h, and the supernatant fluid was corresponded to (c) and (d) with the addition of TMB/H_2O_2 (shown in Fig. 5A). Judged from the supernatant, no escaping of HAb2 was observed when the precipitate of SiO_2@CdSe@SiO_2-HAb2 probes was resuspended in PBS. It can be seen from Fig. 5B that SiO_2@CdSe@SiO_2-HAb2 probes exhibited more obvious color change than individual HAb2. The HAb1 in wells (c) and (d) were incubated with the same concentration of 50 μg mL^{-1} and (e), (a) and (b) with 0, 10, 20 μg mL^{-1}. Obviously, the color in well (d) with SiO_2@CdSe@SiO_2-HAb2 probes is most highlighted. The results showed that the SiO_2@CdSe@SiO_2-HAb2 probes had dramatically amplification capability in ELISA systems.

Fig. 5C and D represented the PL spectrum and SWV measurements before and after acid dissolution with SiO_2@CdSe@SiO_2 probes, respectively. The fluorescence signal was very weak when Rhod-5N (4 μM) mixed with SiO_2@CdSe@SiO_2 probes before acid dissolution. However, the PL intensity increase significantly as Rhod-5N (4 μM) mixed with SiO_2@CdSe@SiO_2 probes after acid dissolution, and the signal change appeared the same in SWV measurements. These facts indicated that Rhod-5N fluorescence and SWV current were amplified by the released Cd^{2+} after acid dissolution as illustrated in Fig. 1B.

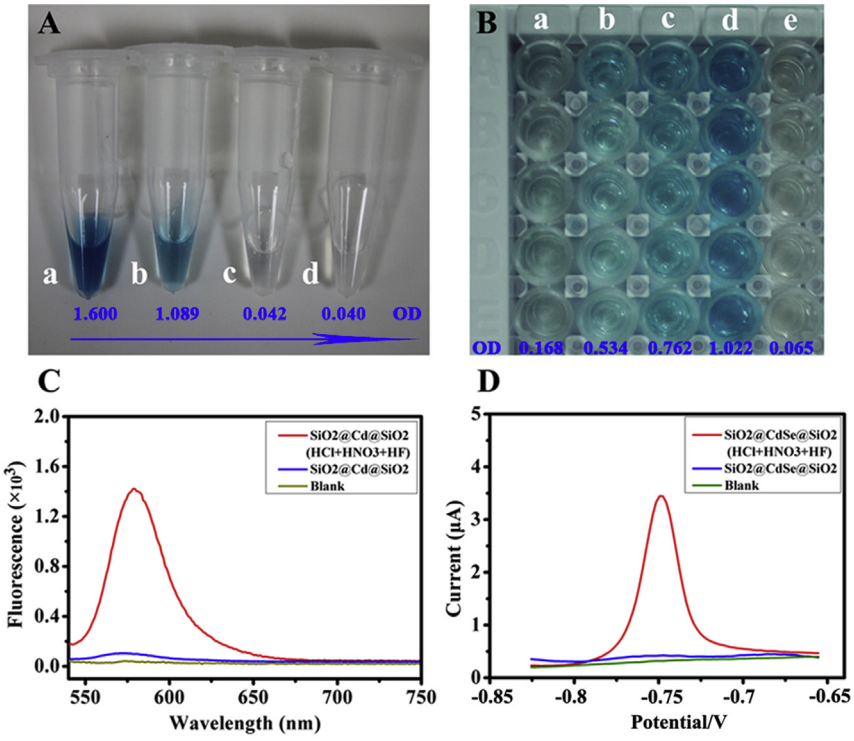

Fig. 5. (A) The stability and of the conjugation: (a) SiO_2@CdSe@SiO_2-HAb_2, (b) HAb_2, the supernatant fluid after immobilization of HAb2 for (c) 24 h and (d) 72 h. (B) Comparison of SiO_2@CdSe@SiO_2-HAb_2 (d) and HAb_2 (a, b, c, e) (concentrations of HAb_1 from (a) to (e): 10, 20, 50, 50, 0 μg mL^{-1}, and six wells for each concentration). (C) The PL spectrum of Rhod-5N (4 μM) with SiO_2@CdSe@SiO_2 probes before and after acid dissolution (v/v, HNO_3: HF: HCl = 1:1:3). (D) SWV measurements of SiO_2@CdSe@SiO_2 probes before and after acid dissolution (v/v, HNO_3: HF: HCl = 1:1:3).

3.3. Optimization of the signal generated by Cd^{2+}

As the CdSe QDs were embedded under the silica shell, a mixed acid solution of HCl–HNO_3–HF was adopted to dissolve the SiO_2@CdSe@SiO_2 probes to release Cd^{2+}. As shown in Fig. 6A and B, different ratios of acid solution mixed with the same concentration of silica probes (1.8 mg mL^{-1}) were discussed via SWV measurements and PL spectrum, and the results showed the ratio of 1:1:3 (HNO_3: HF: HCl) behaved strongest current signal (curve e) and PL intensity (curve e). The results revealed that the amount of Cd^{2+} reached maximum as the ratio of acid solution is 1:1:3, which was finally adopted as the optimal ratio of HNO_3–HF–HCl acid solution.

Owning to the intramolecular photoinduced electron transfer (PET), Rhod-5N normally has very low fluorescence signal (see b in Fig. 1B). However, the PET process is reduced as Rhod-5N bounded with Cd^{2+}, which leads to a great enhancement of the PL intensity [30]. Therefore, Rhod-5N was adopted as sensitive fluorescent probe to recognize Cd^{2+} in the experiment. Nevertheless, the concentration of Rhod-5N greatly influenced PL intensity. As exhibited in Fig. 6C, different concentrations of Rhod-5N to Cd^{2+} (1.0 μM) were investigated in 0.1 M PBS system (pH = 7), and the signal/background ratio increased very slowly as the concentration reached 2 μM and tend to be balanced at 3 μM. Thus, 3 μM of Rhod-5N was adopted in the following experiments.

As the PET process of Rhod-5N largely related to pH [20,31], the fluorescence of Rhod-5N bounded with Cd^{2+} in different pH was explored. It can be seen from Fig. 6D that the PL intensity of Rhod-5N itself changed with pH, and reached the maximum as pH was 7.0. Moreover, in different pH systems, the response of Rhod-5N (3 μM) to Cd^{2+} increased with the increasing Cd^{2+} and appeared to be balanced after Cd^{2+} was added up to 3 μM. However, compared to the PL intensity at pH = 7.0, it reduced dramatically as pH value was too high (10.0) or too low (4.5). These results are probably related to the H^+ or OH^- which blocked the chelation of Rhod-5N with Cd^{2+}. Briefly, the excess H^+ could be in competition with Cd^{2+} for the vacant orbital of oxygen in Rhod-5N, and the excess OH^- may combine with Cd^{2+} to produce $Cd(OH)_2$. Therefore, the high pH promotes the PET process and the low pH reduces the concentration of Cd^{2+}, which weaken the fluorescence signal. Finally, the pH of Rhod-5N bounded with Cd^{2+} was chosen as 7.0 in the following experiments.

3.4. Signal amplification for the detection of HIgG

The results of the amplified assay using SiO_2@CdSe@SiO_2-HAb2 performed on the 96 well plates were shown in Fig. 7B and compared with the conventional assays (Fig. 7A). Both systems behaved good linearity between OD450 and the logarithmic value of the tested ranges of HIgG concentration. The linear regression equation in Fig. 7A was presented as Y1 = −0.148 + 0.220 lg X (X: ng mL^{-1}) over the range from 20 ng mL^{-1} to 20 μg mL^{-1} with R^2 = 0.9725, and the detection limit was calculated to be 19.8 ng mL^{-1} (S/N = 3). Fig. 7B exhibited a regression equation of Y2 = −0.025 + 0.269 lg X (X: ng mL^{-1}) over the range from 5 ng mL^{-1} to 20 μg mL^{-1} with R^2 = 0.9903, and showed a detection limit of 3.9 ng mL^{-1} (S/N = 3). Clearly, the sensitivity of the enzyme-loaded method was 5 times higher than that of the traditional method and possessed a wider linear range.

Fig. 7C showed the current response as a function of HIgG concentration. To further investigate the sensitivity of the SWV measurements, we discussed the peak current with the concentration of HIgG (inset of Fig. 7C). The results revealed that the current increased with the increase of HIgG concentration and showed a linear response to the HIgG in the range of 0.05–20 ng mL^{-1}. The regression equation was Y3 = −24.77 + 13.77 lg X (X: pg mL^{-1}) with R^2 = 0.9779, and the detection limit was 0.05 ng mL^{-1} (S/N = 3). Fig. 7D revealed the PL intensity respond to the different concentrations of HIgG. The response concentration to HIgG was covered from 0.05 to 20 ng mL^{-1} and showed a good linearity over the range of 0.1–20 ng mL^{-1}. The regression equation was expressed as Y4 = −333.07 + 183.83 lg X (X: pg mL^{-1}) with R^2 = 0.9902, and the detection limit was 0.1 ng mL^{-1} (S/N = 3).

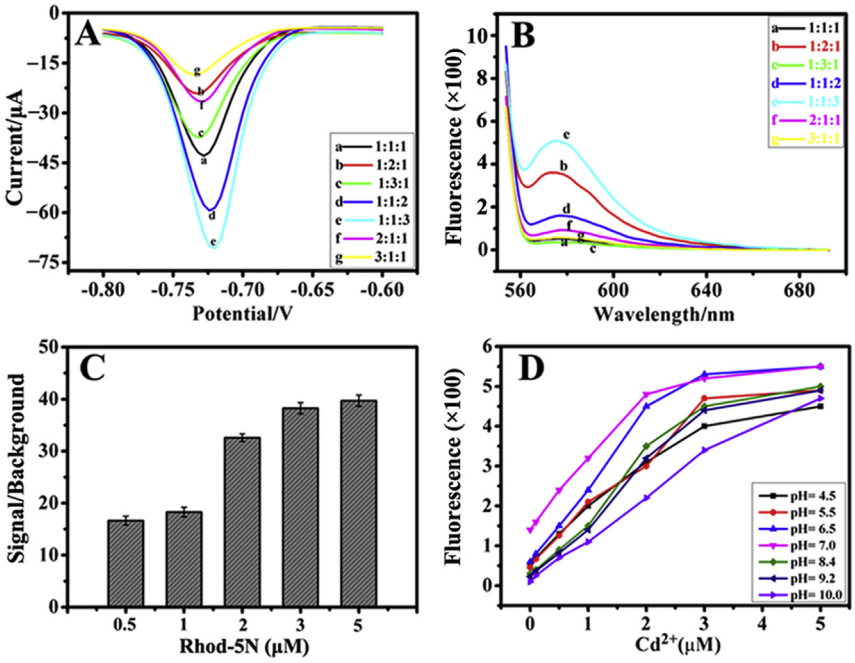

Fig. 6. Optimization results of immunosensor. (A) The results of different ratios of acid solution (HNO_3: HF: HCl) in SWV measurements and (B) PL spectrum. (C) Comparison of the signal (Cd^{2+} = 1.0 μM)/background (Cd^{2+} = 0 μM) ratio with 0.5, 1.0, 2.0, 3.0 and 5.0 μM Rhod-5N in 0.1 M PBS (pH = 7). (D) The detection of Cd^{2+} using Rhod-5N in PBS system with different pH.

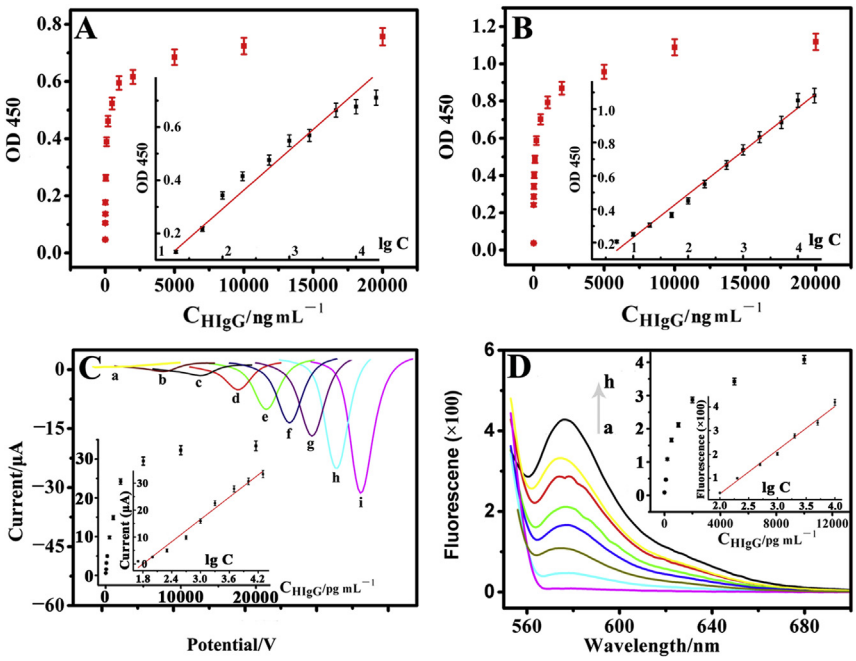

Fig. 7. (A) Conventional ELISA detection of HIgG using TMB/H_2O_2 as substrates (Inset: linear calibration plot between optical density and HIgG concentration). (B) Amplified assay using SiO_2@CdSe@SiO_2-HAb_2 as probes (Inset: the amplified results correspond to A). (C) Current response to 0, 50, 100, 200, 500, 1000, 2000, 5000, 10000 and 20000 pg mL^{-1} HIgG (from a to i) (Inset: linear relationship between SWV current and HIgG concentration ranging from 50 to 20000 pg mL^{-1}). (D) PL intensity response to 0, 100, 200, 500, 1000, 2000, 5000 and 10000 pg mL^{-1} HIgG (from a to h) (Inset: linear relationship between PL intensity and HIgG concentration ranging from 100 to 10000 pg mL^{-1}). All the error bars were calculated based on the standard deviation of three measurements.

Compared with the routine ELISA system (Fig. 7A), 5-fold, 200-fold, and 400-fold increases in sensitivity were obtained for amplified ELISA, PL, and SWV, respectively. The results demonstrated that the SiO_2@CdSe@SiO_2 probes possessed much higher sensitivity than traditional ELISA and some other reported techniques [32–34]. Also, SWV behaved lower detection limit than PL. What's more, the ELISA-based three techniques could corroborate one another and thus enhance the detection reliability. The comparison of the proposed method and the previously published reports for HIgG determination was listed in Table S1.

Also, we found that the probes remained nearly 97% of original PL and current response after 15 days of storage in 10 mM sodium borate buffer solution (SBBS, pH = 9.18) at 4 °C, indicating the good stability of the probes. The activity of the probes was tested after 30 days of storage at 4 °C, which showed good catalytic and immunological activity (see Fig. S3). Furthermore, we investigated the reproducibility of the immunosensor for HIgG with intra-assay precision, which was evaluated by determining one HIgG level for six measurements. The variation coefficients acquired from 20 ng mL^{-1} HIgG was 4.8% for amplified ELISA, 4.2% for SWV assay, and 3.7% for fluorometry. The obtained results demonstrated acceptable reproducibility of the three techniques.

3.5. Detection of PCV2 antibody with SiO_2@CdSe@SiO_2 probes

To evaluate the performance of the SiO_2@CdSe@SiO_2 probes in actual swine serum samples, a series of positive serum samples with different dilution ratios were tested using the proposed system. The results confirmed that the probes had an excellent capability in response to changes of the actual serum samples.

Fig. 8A shows the optical density of conventional ELISA assay for PCV2 antibody in positive swine serum samples at different dilution ratios. The inset standard calibration curve showed a linear regression equation Y5 = 0.746 + 0.166 lg X (X: dilution ratio) ranging from 1:10^2 to 5:10^5 with R^2 = 0.9638 (S/N = 3). After the amplified assay using enzyme-loaded silica as probes, the optical density and linearity range were improved as shown in Fig. 8B and exhibited a regression equation of Y6 = 1.194 + 0.221 lg X (X: dilution ratio) over the range from 1:10^2 to 5:10^6 with R^2 = 0.9813 (S/N = 3). It can be concluded that the SiO_2@CdSe@SiO_2-amplified ELISA system possessed lower level of sensitivity and wider linear range. The results were consistent with the colorimetric detection and the signal was amplified by ~2 order of magnitude even judged by naked eye (as shown Fig. S4).

Under the optimized conditions, the SWV and PL behaviors of the probes for the detection of PCV2 antibody were also investigated. Fig. 8C showed the SWV current response to different dilution ratios of PCV2 antibody. The current intensity gradually decreased with decreasing concentrations of PCV2 antibody, demonstrating the good capability in response to target changes. The standard calibration curve for detection of PCV2 antibody was described in Fig. 8D. The linear regression equation is Y7 = 23.36 + 2.79 lg X (X: dilution ratio) ranging from 1:10^2 to 5:10^7 with R^2 = 0.9623 (S/N = 3). Fig. 8E revealed the relationship between fluorescence intensity and the PCV2 antibody concentration. The fluorescence intensity to PCV2 antibody behaved the same tendency as current intensity. Fig. 8F displayed standard calibration curve of the linear regression equation Y8 = 22.73 + 2.75 lg X (X: dilution ratio) ranging from 1:10^2 to 5:10^7 with R^2 = 0.9618 (S/N = 3). The results indicated that the detection sensitivity of PCV2 antibody was enhanced 100-fold by SWV and PL measurements due to the coated Cd^{2+} signal.

Furthermore, the specificity of the amplified probes for the clinical samples was investigated by contrasting PCV2 positive serum with PCV2 negative serum, pooled serum (positive serum/negative serum = 1:1), pseudorabies virus (PrV) positive serum, porcine reproductive and respiratory syndrome (PRRS) positive serum, HIgG and BSA. As shown in Fig. 9, the stronger optical

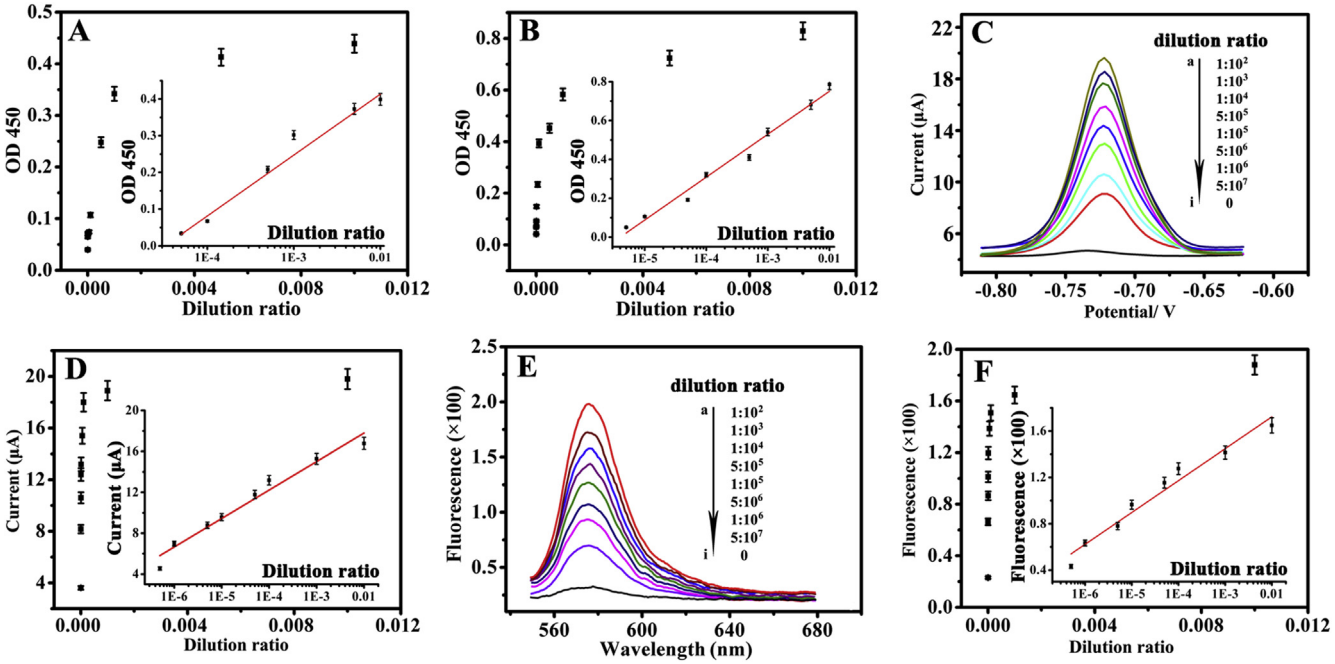

Fig. 8. (A) Conventional ELISA detection of PCV2 antibody using TMB/H_2O_2 as substrates (Inset: linear calibration plot between optical density and different dilution ratios of PCV2 positive serum: $1:10^2$, $5:10^3$, $1:10^3$, $5:10^4$, $1:10^4$, $5:10^5$). (B) Amplified assay using SiO_2@CdSe@SiO_2-PAb_2 as probes (Inset: the amplified results of different dilution ratios of PCV2 positive serum: $1:10^2$, $5:10^3$, $1:10^3$, $5:10^4$, $1:10^4$, $5:10^5$, $1:10^5$, $5:10^6$). (C) Current response to different dilution ratios of PCV2 antibody (a) $1:10^2$, (b) $1:10^3$, (c) $1:10^4$, (d) $5:10^5$, (e) $1:10^5$, (f) $5:10^6$, (g) $1:10^6$, (h) $5:10^7$, (i) 0. (D) Plots of SWV current vs PCV2 antibody in positive serum (Inset: linear relationship between SWV current and different concentrations of PCV2 antibody). (E) PL intensity response to different dilution ratios of PCV2 antibody (a) $1:10^2$, (b) $1:10^3$, (c) $1:10^4$, (d) $5:10^5$, (e) $1:10^5$, (f) $5:10^6$, (g) $1:10^6$, (h) $5:10^7$, (i) 0. (F) Plots of PL density vs PCV2 antibody in positive serum (Inset: linear relationship between PL intensity and different concentrations of PCV2 antibody). All the error bars were calculated based on the standard deviation of three measurements.

densities were acquired for PCV2 positive serum and the pooled serum and nearly no signals appeared for PCV2 negative serum, PrV, PRRS, HIgG and BSA. In addition, the two stronger signals were fitted to the linear regression equation in Fig. 8B. The results testified that the PCV2 antibody can be effectively recognized by the proposed amplification method with high specificity.

4. Conclusions

In this work, great efforts were made to explore the feasibility of a versatile ELISA based immunoassay and achieve an improvement in the detection limit of PCV2 antibody. With HRP enzyme and functionalized silica nanospheres for signal amplification, a versatile label was successfully developed to detect PCV2 antibody based on ELISA. Compared with the traditional ELISA, the proposed strategy exhibited a higher sensitivity and wider linear range. Furthermore, the amplified ELISA system could be used by coupling with other techniques and provide a universal amplification probes for detecting other biological samples. In particular, the proposed strategy would open another avenue on the design of ELISA-based sensors and intrigue researchers into gaining a new interest in the development of ELISA.

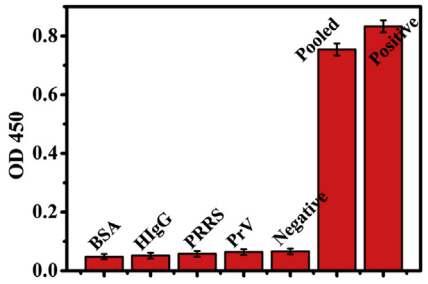

Fig. 9. Specificity of BSA, HIgG, PRRS, PrV, PCV2 negative serum, pooled serum (PCV2 positive serum/PCV2 negative serum = 1:1), and PCV2 positive serum using amplified ELISA system.

Acknowledgments

We gratefully acknowledge the financial support from National Natural Science Foundation of China (21375043, 21175051).

Appendix A. Supplementary data

Supplementary information related to this article can be found at http://dx.doi.org/10.1016/j.aca.2015.06.024.

References

[1] T. Opriessnig, X.J. Meng, P.G. Halbur, J. Vet. Diagn. Invest. 19 (2007) 591–615.
[2] X.J. Meng, Annu. Rev. Anim. Biosci. 1 (2013) 43–64.
[3] S.K. Vashist, J.H.T. Luong, Biosens. Bioelectron. 67 (2015) 73–78.
[4] P.W. Marinelli, M. Lam, L. Bai, R. Quirion, C.A. Gianoulakis, Clin. Exp. Res. 30 (2006) 982–990.
[5] E. Macy, B. Goldberg, K.Y.T. Poon, Ann. Allerg. Asthma Immunol. 105 (2010) 136–141.
[6] N. Ismail, G.E. Fish, M.B. Smith, J. Clin. Microbiol. 42 (2004) 610–617.
[7] F. Shao, Z. Lu, C. Liu, H. Han, K. Chen, W. Li, Q. He, H. Peng, J. Chen, Appl. Mater. Inter. 6 (2014) 6281–6289.
[8] W. Sun, K. Jiao, S. Zhang, C. Zhang, Z. Zhang, Anal. Chim. Acta 434 (2001) 43–50.
[9] Z. Qu, H. Xu, P. Xu, K. Chen, R. Mu, J. Fu, H. Gu, Anal. Chem. 86 (2014) 9367–9371.
[10] J.M. Nam, C.S. Thaxton, C.A. Mirkin, Science 301 (2003) 1884–1886.
[11] H. Yin, Y. Zhou, H. Zhang, X. Meng, S. Ai, Biosens. Bioelectron. 33 (2012)

247–253.
[12] R.J. Davenport, G.J.L. Wuite, R. Landick, C. Bustamante, Science 287 (2000) 2497–2500.
[13] G.J.L. Wuite, R.J. Davenport, A. Rappaport, C. Bustamante, Biophys. J. 79 (2000) 1155–1167.
[14] K. Ren, J. Wu, Y. Zhang, F. Yan, H. Ju, Anal. Chem. 86 (2014) 7494–7499.
[15] J. Wang, H. Han, X. Jiang, L. Huang, L. Chen, N. Li, Anal. Chem. 84 (2012) 4893–4899.
[16] H. Wang, C. Zheng, T. Dong, K. Liu, H. Han, J. Liang, J. Phys. Chem. C 117 (2013) 3011–3018.
[17] L. Chen, C. Chen, R. Li, Y. Li, S. Liu, Chem. Commun. 19 (2009) 2670–2672.
[18] D. Xiang, G. Zeng, Z. He, Biosens. Bioelectron. 26 (2011) 4405–4410.
[19] J. Qian, C. Zhang, X. Cao, S. Liu, Anal. Chem. 82 (2010) 6422–6429.
[20] X.P. Li, K. Chen, L. Huang, D.L. Lu, J.G. Liang, H.Y. Han, Microchim. Acta 180 (2013) 303–310.
[21] L. Huang, Q. Wu, J. Wang, M. Foda, J. Liu, K. Cai, H. Han, Chem. Commun. 50 (2014) 2896–2899.
[22] K. Muzyka, Biosens. Bioelectron. 54 (2014) 393–407.
[23] B.H. Jun, D.W. Hwang, H.S. Jung, J. Jang, H. Kim, H. Kang, T. Kang, S. Kyeong, H. Lee, D.H. Jeong, K.W. Kang, H. Youn, D.S. Lee, Y.S. Lee, Adv. Funct. Mater. 22 (2012) 1843–1849.
[24] G. Lai, J. Wu, C. Leng, H. Ju, F. Yan, Biosens. Bioelectron. 26 (2011) 3782–3787.
[25] W. Stöber, A. Fink, E. Bohn, J. Colloid. Interf. Sci. 26 (1968) 62–69.
[26] L.M. Liz-Marzán, M. Giersig, P. Mulvaney, Langmuir 12 (1996) 4329–4335.
[27] Y. Wu, C. Chen, S. Liu, Anal. Chem. 81 (2009) 1600–1607.
[28] J.J. Zhang, T.T. Zheng, F.F. Cheng, J.J. Zhu, Chem. Commun. 47 (2011) 1178–1180.
[29] C. Chen, Y. Li, S. Liu, J. Electroanal. Chem. 632 (2009) 14–19.
[30] M. Soibinet, V. Souchon, I. Leray, B. Valeur, J. Fluoresc. 18 (2008) 1077–1082.
[31] P. Goswami, D.K. Das, J. Fluoresc. 22 (2012) 391–395.
[32] D. Tian, C. Duan, W. Wang, N. Li, H. Zhang, H. Cui, Y. Lu, Talanta 78 (2009) 399–404.
[33] R.J. Cui, J.J. Zhu, Electrochim. Acta 55 (2010) 7814–7817.
[34] C.F. Duan, Y.Q. Yu, H. Cui, Analyst 133 (2008) 1250–1255.

List of abbreviations

ELISA: Enzyme–linked immunosorbent assay
PRV2: Pseudorabies virus type 2
SWV: square-wave voltammetry
QDs: Quantum
HIgG: Human IgG
PCVAD: porcine circovirus-associated disease
PCVD: porcine circovirus disease
FEIA: fluorometric enzyme immunoassay
SERS: Surface enhanced Raman scattering
PrV: porcine pseudorabies virus
PAb2: PCV2 secondary antibody
TEOS: Tetraethyl orthosilicate
GPTMS: 3-(Glycidyloxypropyl) trimethoxysilane
MPTS: (3-Mercaptopropyl) trimethoxysilane
BSA: bovine serum albumin
HDA: hexadecylamine
SA: stearic acid
DOA: dioctylamine
MPA: mercaptopropionic acid
OTMS: N-octyltrimethoxysilane
Rhod-5N: Rhodamine 5 N
HIgG: Human IgG antigen
HAb1: rabbit anti-human IgG antibody
HAb2: HRP-conjugated goat anti-human IgG antibody
PAb1: PCV2 antibody
PAb2: HRP-conjugated rabbit anti-pig IgG antibody
PRRS: Porcine Reproductive and Respiratory syndrome
PL: Photoluminescence